

# Experimental investigation of the alluaudite + triphylite assemblage, and development of the Na-in-triphylite geothermometer: applications to natural pegmatite phosphates

Frederic Hatert · Luisa Ottolini ·  
Peter Schmid-Beurmann

Received: 4 February 2010 / Accepted: 15 June 2010 / Published online: 7 July 2010  
© Springer-Verlag 2010

**Abstract** In order to assess the stability of the primary alluaudite + triphylite assemblage, we performed hydrothermal experiments between 400 and 800°C, starting from the  $\text{LiNa}_2\text{Mn}_x\text{Fe}_{3-x}^{2+}\text{Fe}^{3+}(\text{PO}_4)_4$  compositions ( $x = 1.054, 1.502, 1.745$ ) that represent the ideal compositions of the alluaudite + triphylite assemblages from the Kibingo (Rwanda), Hagendorf-Süd (Germany), and Buranga (Rwanda) pegmatites, respectively. The pressure was maintained at 1 kbar, and the oxygen fugacity was controlled by the Ni–NiO buffer. The results of these experiments show that the alluaudite + triphylite assemblage crystallizes at 400 and 500°C, while the association alluaudite + triphylite + marićite appears at 600 and 700°C. The limit between these two domains, at ca. 550°C, corresponds to the maximum temperature that can be reached by the alluaudite + triphylite assemblages in granitic pegmatites, because marićite has never been observed in such geological environments. At 800°C, the

formation of the X-phase + triphylite assemblage indicates a strong reduction of the bulk composition, according to the reaction  $0.5\text{LiM}^{2+}\text{PO}_4$  (triphylite) +  $3\text{Na}_2\text{M}_2^{2+}\text{Fe}^{3+}(\text{PO}_4)_3$  (alluaudite) +  $1.5\text{H}_2\text{O} = 4.5\text{NaM}^{2+}\text{PO}_4$  (marićite) +  $\text{Li}_{0.5}\text{Na}_{1.5}\text{M}_5^{2+}(\text{PO}_4)_4$  (X-phase) +  $\text{H}_3\text{PO}_4 + 0.75\text{O}_2$  ( $\text{M}^{2+} = \text{Fe}^{2+}, \text{Mn}$ ). Secondary ion mass spectrometry (SIMS) was used at our knowledge for the first time to measure Li in all the Li-bearing phosphates. A specific methodological procedure was developed with the ion microprobe to get accurate  $\text{Li}_2\text{O}$  data over a wide concentration range spanning from few ppm Li up to ~11 wt%  $\text{Li}_2\text{O}$ . Our SIMS analyses of the synthesized phosphates indicate that the Li contents of alluaudites, marićites, and X-phase increase progressively with temperature, while the Li content of triphylite-type phosphates decreases due to the Li → Na substitution. The Na-exchange equilibrium between triphylite-type phosphates and alluaudite is correlated with the temperature according to the equation:  $\ln(x_{\text{Na}}^{\text{Tri}}/x_{\text{Na}}^{\text{All}}) = -7.0(7) \cdot 10^3/T + 5.4(9)$ . This equation can be used to estimate the crystallization temperature of triphylite–alluaudite assemblages independently of the oxygen fugacity.

Communicated by T. L. Grove.

**Electronic supplementary material** The online version of this article (doi:10.1007/s00410-010-0547-6) contains supplementary material, which is available to authorized users.

F. Hatert (✉)  
Laboratoire de Minéralogie, Département de Géologie,  
Bâtiment B18, Université de Liège, 4000 Sart-Tilman, Belgium  
e-mail: fhatert@ulg.ac.be

L. Ottolini  
C.N.R.-Istituto di Geoscienze e Georisorse (IGG),  
Unità di Pavia, Via A. Ferrata 1, 27100 Pavia, Italy

P. Schmid-Beurmann  
Institut für Mineralogie, Corrensstrasse 24,  
48149 Münster, Germany

**Keywords** Alluaudite · Triphylite · Na–Li–Mn–Fe<sup>2+</sup>–Fe<sup>3+</sup> phosphates · Pegmatites · Phase relations · Geothermometry · SIMS

## Introduction

In rare-element pegmatites of the beryl-columbite-phosphate subtype (Černý 1991; Černý and Ercit 2005), Fe–Mn phosphate minerals occur as masses enclosed in silicates, and these masses can reach several meters in diameter. Among these phosphates, minerals of the triphylite–lithiophilite series [ $\text{LiFe}^{2+}(\text{PO}_4)$ – $\text{LiMn}(\text{PO}_4)$ ] are the most

common primary (magmatic) phases. Minerals of the alluaudite group, with ideal chemical compositions ranging from  $\text{Na}_2\text{Mn}(\text{Fe}^{2+}\text{Fe}^{3+})(\text{PO}_4)_3$  to  $\square\text{NaMnFe}_2^{3+}(\text{PO}_4)_3$ , are generally produced from primary triphylite–lithiophilite, by oxidation coupled with a  $\text{Li} \rightarrow \text{Na}$  metasomatic exchange process. Several occurrences of such secondary alluaudites were reported by Huvelin et al. (1972), Fransolet (1975), Fontan et al. (1976), Fontan (1978), Boury (1981), Lahti (1981), Fransolet et al. (1985, 1986), Keller and Von Knorring (1989), Roda et al. (1996), and Roda Robles et al. (1998).

The existence of primary alluaudites, first alluded to Fisher (1958) in his presidential address to the Mineralogical Society of America, was confirmed by Fransolet (1975, 1977), who noted sharp contacts between alluaudite and ferrisicklerite  $[\text{Li}_{1-x}(\text{Fe}^{3+},\text{Mn}^{2+})\text{PO}_4]$  from the Buranga pegmatite, Rwanda, without any replacement texture. This observation indicates that the metasomatic replacement process proposed by Moore (1971) cannot be generalized. Héreng (1989) re-examined the samples from the Buranga pegmatite and observed three different primary assemblages: alluaudite + triphylite, alluaudite + fillowite  $[\text{Na}_2\text{Ca}(\text{Mn},\text{Fe}^{2+})_7(\text{PO}_4)_6]$ , and alluaudite + arrojadite  $[(\text{KNa})\text{Fe}^{2+}(\text{CaNa}_2)\text{Fe}_{13}^{2+}\text{Al}(\text{PO}_4)_{11}(\text{PO}_3\text{OH})(\text{OH})_2]$ . More recently, Fransolet et al. (1994, 1997, 1998, 2004) observed several assemblages involving primary alluaudites: alluaudite + arrojadite in Hagendorf-Süd, Germany; alluaudite + fillowite in Rusororo, Rwanda, and Kabira, Uganda; alluaudite + ferrisicklerite + heterosite  $[(\text{Fe}^{3+},\text{Mn}^{3+})\text{PO}_4]$  in Kibingo and Wasurenge, Rwanda.

As observed for the phosphates of the triphylite–lithiophilite series, which progressively transform to ferrisicklerite–sicklerite  $[\text{Li}_{1-x}(\text{Fe}^{3+},\text{Mn}^{2+})(\text{PO}_4)-\text{Li}_{1-x}(\text{Mn}^{2+},\text{Fe}^{3+})(\text{PO}_4)]$  and to heterosite–purpurite  $[(\text{Fe}^{3+},\text{Mn}^{3+})(\text{PO}_4)-(\text{Mn}^{3+},\text{Fe}^{3+})(\text{PO}_4)]$  due to oxidation and Li-leaching, the primary alluaudites, which are weakly oxidized, progressively transform into oxidized secondary alluaudites. In order to maintain charge balance, Na is leached out of the alluaudite crystal structure, according to the substitution mechanism  $\text{Na}^+ + \text{Fe}^{2+} \rightarrow \square + \text{Fe}^{3+}$ , as observed by Mason (1941) and Fransolet et al. (1984, 1985, 2004). This oxidation mechanism, coupled with Na leaching, explains the transformation of hagendorfite  $[\text{Na}_2\text{MnFe}^{2+}\text{Fe}^{3+}(\text{PO}_4)_3]$  into alluaudite  $[\square\text{NaMnFe}_2^{3+}(\text{PO}_4)_3]$ , and of ferrohagendorfite  $[\text{Na}_2\text{Fe}_2^{2+}\text{Fe}^{3+}(\text{PO}_4)_3]$  into ferroalluaudite  $[\square\text{NaFe}^{2+}\text{Fe}_2^{3+}(\text{PO}_4)_3]$ .

Since the petrogenetic importance of accessory phosphates has been demonstrated in the ultrahigh-pressure rocks of the Dora-Maira massif, Italy (Brunet et al. 1998), it now clearly appears that experimental studies on these rare minerals are necessary to better understand the genesis of pegmatites (London et al. 1999, 2001). With this goal in mind, Hatert et al. (2006) investigated the

$\text{Na}_2(\text{Mn}_{1-x}\text{Fe}_x^{2+})_2\text{Fe}^{3+}(\text{PO}_4)_3$  series ( $x = 0\text{--}1$ ), which models the chemical compositions of natural, weakly oxidized, primary alluaudites. For this purpose, hydrothermal experiments were performed between 400 and 800°C, at 1 kbar and under oxygen fugacities controlled by the  $\text{Ni}-\text{NiO}$ ,  $\text{Fe}_2\text{O}_3-\text{Fe}_3\text{O}_4$ ,  $\text{Cu}_2\text{O}-\text{CuO}$ , and  $\text{Fe}-\text{Fe}_3\text{O}_4$  buffers. The authors showed that under the oxygen fugacity controlled by the  $\text{Ni}-\text{NiO}$  buffer, single-phase alluaudites crystallize at 400 and 500°C, whereas the association alluaudite + marićite  $[\text{NaFe}^{2+}\text{PO}_4]$  appears between 500 and 700°C. The limit between these two fields corresponds to the maximum temperature that can be reached by alluaudites in granitic pegmatites, because marićite has never been observed in such geological environments.

In order to corroborate the existence of primary alluaudite + triphylite assemblages in pegmatites, we decided to perform hydrothermal experiments between 400 and 800°C, at 1 kbar and under an oxygen fugacity controlled by the  $\text{Ni}-\text{NiO}$  buffer, starting from the ideal compositions of the alluaudite + triphylite (or heterosite) assemblages from the Buranga, Kibingo (Rwanda), and Hagendorf-Süd (Germany) pegmatites. The aim of this paper is to report the results of these experiments, which will provide a tool for constraining the temperature that prevailed in pegmatites during the crystallization of the alluaudite + triphylite assemblage.

## Experimental procedure

The hydrothermal experiments were performed between 400 and 800°C at 1 kbar, starting from compositions  $\text{LiNa}_2\text{Mn}_x\text{Fe}_{3-x}^{2+}\text{Fe}^{3+}(\text{PO}_4)_4$  ( $x = 1.054, 1.502, 1.745$ ), which represent the ideal compositions of the alluaudite + triphylite assemblages from the Kibingo, Hagendorf-Süd, and Buranga pegmatites, respectively. These starting compositions were calculated from the  $\text{Fe}/(\text{Fe} + \text{Mn})$  ratio measured on natural assemblages (Boury 1981; Héreng 1989; Fransolet et al. 2004), assuming that the primary phosphates were weakly oxidized, and that they occurred in a 1:1 M ratio. Stoichiometric quantities of  $\text{NaH}_2\text{PO}_4 \cdot \text{H}_2\text{O}$  (Merck, Darmstadt, Germany, min. 99%),  $\text{LiOH} \cdot \text{H}_2\text{O}$  (Riedel-de-Haën, Germany, min. 98%),  $\text{Mn}_2\text{P}_2\text{O}_7$ ,  $\text{MnO}$  (Alfa, Karlsruhe, Germany, 99.5%),  $\text{FePO}_4$ , and  $\text{FeO}$  (Aldrich, Steinheim, Germany, 99%) were homogenized in a mortar under acetone, in order to prevent oxidation of  $\text{FeO}$ .  $\text{FePO}_4$  was previously synthesized by solid-state reaction in air, starting from a stoichiometric mixture of  $\text{NH}_4\text{H}_2\text{PO}_4$  (Merck, min. 99%) and  $\text{FeSO}_4 \cdot 7\text{H}_2\text{O}$  (Merck, min. 99.5%), which was heated in a platinum crucible at 900°C for 1 day.  $\text{Mn}_2\text{P}_2\text{O}_7$  was obtained by heating  $\text{MnHPO}_4 \cdot x\text{H}_2\text{O}$  (Alfa, Karlsruhe, Germany, min. 99%) in a platinum crucible at

900°C during a few hours. The purity of both FePO<sub>4</sub> and Mn<sub>2</sub>P<sub>2</sub>O<sub>7</sub> was checked by X-ray powder diffraction.

Approximately 20–30 mg of the starting material was welded, together with 2 µl of distilled water, into small Ag<sub>70</sub>Pd<sub>30</sub> tubes with an outer diameter of 2 mm, a wall thickness of 0.1 mm and a length of 25 mm. In order to control the oxygen fugacity, a double-capsule device similar to that developed by Eugster (1957) was used. Approximately 100–300 mg of a Ni + NiO homogeneous mixture (NNO oxygen fugacity buffer, O'Neill and Pownceby 1993) was introduced, together with 10 µl of distilled water, into large gold tubes of 4 mm outer diameter, 0.1 mm wall thickness, and 40 mm length. The Ag<sub>70</sub>Pd<sub>30</sub> tubes were then placed in the larger gold tubes which were also welded. The capsules were finally introduced into a conventional hydrothermal apparatus with vertically arranged Tuttle-type cold-seal bombs (Tuttle 1949) for 7 days and then cooled in a stream of cold air. Pressure and temperature errors are estimated to be within ±3% and ±10°C, respectively. After the experiment, the buffer was examined by X-ray powder diffraction, in order to check if the mixture was still present. A few synthesis experiments were also performed without control of the oxygen fugacity; the starting material was then welded with 2 µl of water into small gold tubes with an outer diameter of 2 mm, a wall thickness of 0.1 mm, and a length of 25 mm.

## Analytical procedures

The powder X-ray diffraction patterns of the synthesized compounds were recorded on a Philips PW-3710 diffractometer using 1.9373 Å FeK $\alpha$  radiation. The unit-cell parameters were calculated with the LCLSQ 8.4 least-squares refinement program (Burnham 1991) from the *d*-spacings calibrated with Pb(NO<sub>3</sub>)<sub>2</sub> as an internal standard.

Electron-microprobe analyses of natural and synthetic phosphates were performed with a Cameca SX-50 instrument located in Bochum, Germany (analyst H.-J. Bernhardt), which operated in the wavelength-dispersion mode with an accelerating voltage of 15 kV and a beam current of 15 nA. The standards used were graftonite from Kabira (sample KF16, Fransolet 1975) (for Fe, Mn, P), pyrope (Mg, Al, Si), ZnO (Zn), andradite (Ca), jadeite (Na), and a K-glass (K). The formulae of triphylite, marićite, alluaudite, and X-phase [(Na,Li)<sub>2</sub>(Fe<sup>2+</sup>,Mn)<sub>5</sub>(PO<sub>4</sub>)<sub>4</sub>] were calculated on the basis of 1, 1, 3, and 4 P, respectively, and the FeO and Fe<sub>2</sub>O<sub>3</sub> contents were then calculated to maintain charge balance. No evidence of sodium migration under the electron beam was observed; the analyses of synthetic phosphates are reproducible and in good agreement with those given by Hatert et al. (2006).

SIMS measurements were performed with a Cameca IMS 4f ion microprobe installed at CNR-IGG, Pavia (Italy). We used a 12.5-kV accelerated <sup>16</sup>O<sup>−</sup> primary-ion beam with a current intensity in the range 0.8–4 nA, corresponding to a beam diameter of ~3–6 µm. The samples were polished, washed in an ultrasonic tank with ethanol, and Pt coated (400 Å thickness) before analysis. Secondary ion signals of the following isotopes <sup>6</sup>Li<sup>+</sup>, <sup>31</sup>P<sup>+</sup>, and <sup>57</sup>Fe<sup>+</sup> were detected at the electron multiplier. Acquisition times were 3 s for Li and P (each), and 6 s for Fe over 3 cycles. The time required to reach steady emission (waiting time) under the employed experimental set up has been 360 s. In the present work, all measurements were done under steady state sputtering conditions, i.e., after waiting 360 s under static (raster zero) ion beam bombardment (~75–125 eV secondary ions) before starting “true” analysis. As it was demonstrated (Ottolini et al. 1993, 2002 and reference therein), the use of medium-to-high-energy (*energy filtering*) secondary ions reduces matrix effects affecting light-element ionization and improves the reproducibility of analysis.

We used triphylite from the Buranga pegmatite, Rwanda, as reference material for Li. The wet-chemical analysis of this sample is given in Héreng (1989), and it contains 9.96 wt% Li<sub>2</sub>O. The calibration factor for Li in the standard was obtained through the calculation of the experimental Li-ion yield (IY) after choosing P and Fe as the internal elements for the matrix. We derived both the IY(Li/P) and the IY(Li/Fe) for the triphylite standard. We remember here, as an example, the definition of the relative-to-P ion yield of Li, IY(Li/P), as  $(\text{Li}^+/\text{P}^+)/(\text{Li(at)}/\text{P(at)})$  where Li<sup>+</sup>, P<sup>+</sup> are the ion current intensities detected at the electron multiplier and (at) represents the elemental atomic concentration. The two IYs were used to calculate the Li<sub>2</sub>O concentrations (wt%) in the “unknown” compounds. The two Li<sub>2</sub>O concentrations for each sample were thus cross-checked by means of two independent internal references for the matrix: P and Fe.

Considering the samples in this study, the final Li<sub>2</sub>O (wt%) data for each crystal analyzed was averaged between the Li<sub>2</sub>O concentrations obtained by the means of the IY(Li/P) and IY(Li/Fe). Such a SIMS approach allowed for the check of the residual matrix effects (if any), possibly affecting Li/P and Li/Fe over a wide range of Li concentrations as well as the eventual presence of instrumental bias (e.g. shift of the peak, instabilities in the ion current, ...) during analysis. On the basis of the results obtained, we can point out a good agreement between the two Li<sub>2</sub>O concentrations for each sample investigated. The mean of the Li<sub>2</sub>O values, and their standard deviations (1 $\sigma$ ), is reported in the analytical tables. The higher standard deviations generally pertain to the low or very low Li concentrations. In this latter case, fluctuations of the secondary ion signals, governed by Poisson counting statistics, are the main causes responsible

for the scatter. For  $\text{Li}_2\text{O}$  concentration values at the percent level, the analytical uncertainty is always very low, i.e., few percent relative or lower, as 1 st. dev.%.

## Phase characterization

### Alluaudite-type phosphates

Alluaudite-type phosphates have been obtained in all experimental runs below 800°C, and they were frequently associated with other phases (Table 1), mainly triphylite, marićite, and X-phase. At low temperatures of 400 and 500°C, alluaudite crystals show a diameter of 10–20  $\mu\text{m}$ , while at 700°C, the crystals reach 50  $\mu\text{m}$  (Fig. 1a, b). These large crystals are euhedral and show a dark green to brownish pleochroism (Fig. 1a). Electron-microprobe analyses (Table 2) show a correlation between the number of ( $\text{Fe}^{3+}$  + vacancies) per formula unit (*p.f.u.*) and the number of ( $\text{Fe}^{2+}$  + Mn) *p.f.u.*, in agreement with the substitution mechanism  $\text{Mn}^{2+} + 2 \text{Fe}^{2+} \rightarrow \square + 2 \text{Fe}^{3+}$  established by Hatert (2004) and Hatert et al. (2006). The substitution  $\text{Na} \rightarrow \text{Li}$  also allows a significant amount of

lithium to be inserted into the alluaudite structure. If we consider the high values of 0.40 and 0.38 wt%  $\text{Li}_2\text{O}$  (samples H.308 and H.309, respectively) as being influenced by the presence of triphylite in impurities, the  $\text{Li}_2\text{O}$  content of alluaudites ranges from 0.06 wt% at 500°C to 0.22 wt% at 700°C (Table 2).

The crystal structure of alluaudite ( $a = 12.004(2)$ ,  $b = 12.533(4)$ ,  $c = 6.404(1)$  Å,  $\beta = 114.4(1)^\circ$ ,  $C2/c$ ) consists of kinked chains of edge-sharing octahedra stacked parallel to {101} (Moore 1971). These chains are formed by a succession of  $M(2)$  octahedral pairs linked by highly distorted  $M(1)$  octahedra. Equivalent chains are connected in the  $b$  direction by the P(1) and P(2) phosphate tetrahedra to form sheets oriented perpendicular to [010]. These interconnected sheets produce channels parallel to  $c$  that contain the distorted cubic  $A(1)$  site and the  $A(2)'$  site which exhibits a morphology of gable disphenoid. The general structural formula of alluaudite-type phosphates is  $[A(2)A(2)'][A(1)A(1)'A(1)''_2]M(1)M(2)_2(\text{PO}_4)_3$  (Hatert et al. 2000); in natural alluaudites, the large crystallographic  $A$  sites are occupied by  $\text{Na}^+$ ,  $\text{Ca}^{2+}$  or  $\text{Mn}^{2+}$ , and the distorted octahedral  $M$  sites are populated by  $\text{Mn}^{2+}$ ,  $\text{Fe}^{2+}$ ,  $\text{Fe}^{3+}$ ,  $\text{Al}^{3+}$  or  $\text{Mg}^{2+}$  (Moore and Ito 1979).

**Table 1** Results of synthesis experiments on the  $\text{LiNa}_2\text{Mn}_x\text{Fe}_{3-x}^{2+}\text{Fe}^{3+}(\text{PO}_4)_4$  starting compositions ( $x = 1.054, 1.502, 1.745$ )

Starting compositions	T (°C)	P (kbar)	f(O <sub>2</sub> )	Duration (days)	Run products	Run no.
$\text{LiNa}_2\text{Mn}_{1.745}\text{Fe}_{1.255}^{2+}\text{Fe}^{3+}(\text{PO}_4)_4$ ( $x = 1.745$ , Buranga, BU)	400	1	NNO	7	Alluaudite + triphylite	H.146
	400	1	–	7	Alluaudite + triphylite	H.308
	500	1	NNO	7	Alluaudite + triphylite	H.149
	500	1	–	7	Alluaudite + triphylite + marićite	H.299
	600	1	NNO	7	Alluaudite + triphylite + marićite + (Fe,Mn) <sub>3</sub> (PO <sub>4</sub> ) <sub>2</sub> · <i>n</i> H <sub>2</sub> O	H.152
	700	1	NNO	7	Marićite + alluaudite + triphylite + X-phase	H.155
	800	1	NNO	7	X-phase + triphylite	H.158
	400	1	NNO	7	Alluaudite + triphylite	H.147
	400	1	–	7	Alluaudite + triphylite	H.310
	500	1	NNO	7	Alluaudite + triphylite	H.150
$\text{LiNa}_2\text{Mn}_{1.502}\text{Fe}_{1.498}^{2+}\text{Fe}^{3+}(\text{PO}_4)_4$ ( $x = 1.502$ , Hagendorf-Süd, HA)	500	1	–	7	Alluaudite + triphylite	H.301
	600	1	NNO	7	Alluaudite + triphylite + marićite (tr.) + (Fe,Mn) <sub>3</sub> (PO <sub>4</sub> ) <sub>2</sub> · <i>n</i> H <sub>2</sub> O	H.153
	700	1	NNO	7	Alluaudite + triphylite + marićite	H.156
	800	1	NNO	7	X-phase + triphylite	H.159
	400	1	NNO	7	Alluaudite + triphylite	H.148
	400	1	–	7	Alluaudite + triphylite	H.309
	500	1	NNO	7	Alluaudite + triphylite	H.151
	500	1	–	7	Alluaudite + triphylite	H.300
	600	1	NNO	7	Alluaudite + triphylite + marićite + magnetite	H.154
	700	1	NNO	7	Alluaudite + triphylite + marićite	H.157
$\text{LiNa}_2\text{Mn}_{1.054}\text{Fe}_{1.946}^{2+}\text{Fe}^{3+}(\text{PO}_4)_4$ ( $x = 1.054$ , Kibingo, KI)	800	1	NNO	7	X-phase + triphylite	H.160

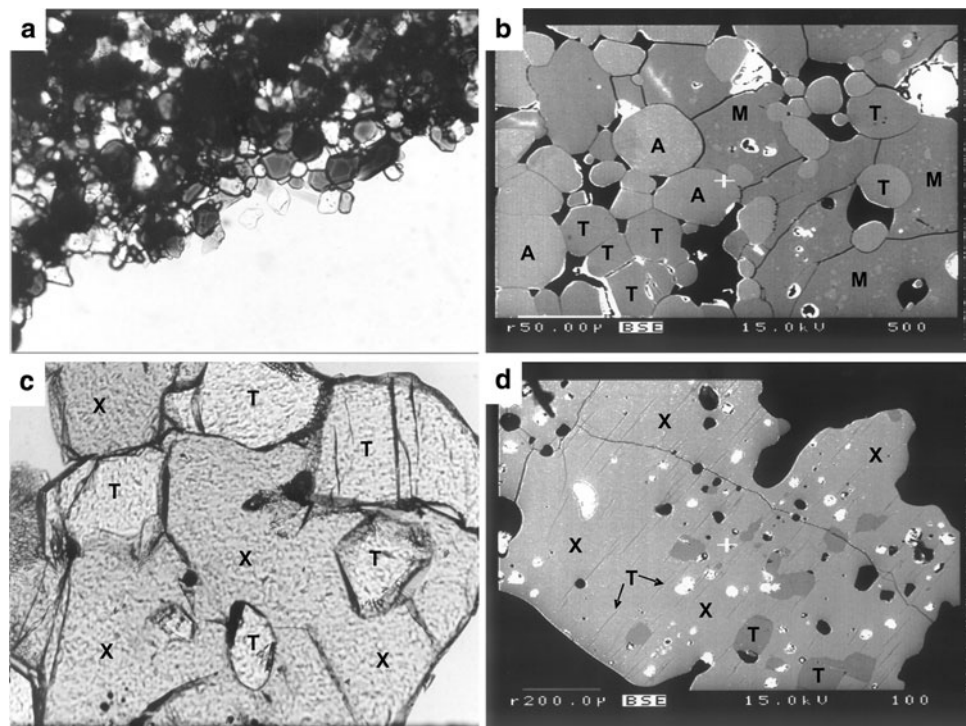


**Fig. 1** **a** Photomicrograph showing euhedral alluaudite crystals (dark grey), associated with marićite and triphyllite grains (colorless). Sample H.157, plane polarized light. The long edge of the photograph is approximately 750 µm. **b** Micrograph showing large grains of marićite (dark grey, M), including smaller grains of alluaudite (light grey, A) and of triphyllite (dark grey, T). Sample H.157, scanning electron microscope, secondary electron image. **c** Photomicrograph

showing a large grain of X-phase (X), containing inclusions of triphyllite (T, colorless). Sample H.159, plane polarized light. The long edge of the photograph is approximately 500 µm. **d** Micrograph showing large grain of X-phase (light grey, X), including inclusions and exsolutions of triphyllite (dark grey, T). Sample H.160, scanning electron microscope, secondary electron image

The unit-cell parameters of some alluaudite-type compounds synthesized in this study are available at Springer's ESM (Electronic Supplementary Material) and are comparable to those measured by Hatert et al. (2006) on alluaudite-type phosphates synthesized in the  $\text{Na}_2(\text{Mn}_{2-2x}\text{Fe}_{1+2x})(\text{PO}_4)_3$  system. The  $\text{Fe}_{\text{total}}/(\text{Fe}_{\text{total}} + \text{Mn})$  ratios, calculated with the correlations established by Hatert et al. (2006) from the  $a$ ,  $b$ , and  $V$  unit-cell parameters of synthetic alluaudites, compare fairly with the  $\text{Fe}_{\text{total}}/(\text{Fe}_{\text{total}} + \text{Mn})$  ratios measured by electron-microprobe (Table 2).

#### Triphyllite-type phosphates

Triphyllite-type phosphates have been observed in all hydrothermal experiments performed in this study, from 400 to 800°C (Table 1). At low temperatures of 400 and 500°C, triphyllite crystals show a diameter of 10–20 µm, comparable to that of alluaudites, while at 700°C, the crystals reach 50 µm (Fig. 1a, b). At 800°C, triphyllite is associated with X-phase and forms rounded crystals reaching 150–200 µm in length (Fig. 1c, d). In runs H.159 and H.160, exsolutions of triphyllite were observed along the cleavage planes of X-phase (Fig. 1d). Electron-microprobe analyses of the run

products (Table 3) show  $\text{Fe}_{\text{total}}/(\text{Fe}_{\text{total}} + \text{Mn})$  ratios from 0.219 to 0.774, corresponding to the compositions of both lithiophilite and triphyllite. Interestingly, a significant amount of Na is observed in the synthetic triphyllite-type phosphates described herein, an amount which evolves from 0.04–0.08 wt%  $\text{Na}_2\text{O}$  at 400°C to 1.25–1.58 wt%  $\text{Na}_2\text{O}$  at 800°C (Table 3). The low Li contents of the Na-rich samples (Table 3) indicate that sodium certainly replaces lithium on the  $M(1)$  site of the structure, following the substitution mechanism  $\text{Na} \rightarrow \text{Li}$ . This first experimental evidence of Na incorporation into triphyllite is not really surprising, since the  $M(1)$  site of the olivine structure can be completely filled by Na in natrophilite (Moore 1972).

Minerals of the triphyllite–lithiophilite series are isostructural with olivine (triphyllite:  $a = 6.092$ ,  $b = 10.429$ ,  $c = 4.738 \text{ \AA}$ ,  $Pmn$ ). Their crystal structure has been investigated from synthetic samples (Geller and Durand 1960; Yakubovich et al. 1977) and natural minerals (Finger and Rapp 1969; Losey et al. 2004) and is characterized by two chains of edge-sharing octahedra parallel to the  $a$  axis. The first chain is constituted by the  $M(1)$  octahedra occupied by Li, while the second chain is formed by the  $M(2)$  sites occupied by Fe and Mn (Fig. 2a). The chains are

**Table 2** Chemical analyses of alluaudite-type phosphates, hydrothermally synthesized from the  $\text{LiNa}_2\text{Mn}_x\text{Fe}^{2+}_{3-x}\text{Fe}^{3+}(\text{PO}_4)_4$  ( $x = 1.054, 1.502, 1.745$ ) starting compositions

Run no.	H.208 (13) BU 400	H.299 (12) BU 500	H.152 (9) BU 700	H.155 (14) BU 700	H.310 (10) HA 400	H.301 (9) HA 500	H.153 (11) HA 600	H.156 (9) HA 700	H.309 (7) KI 400	H.300 (7) KI 500	H.154 (7) KI 600	H.157 (14) KI 700
P <sub>2</sub> O <sub>5</sub>	43.21	43.06	42.96	42.95	43.68	43.43	43.23	43.48	43.87	42.93	42.73	42.56
Fe <sub>2</sub> O <sub>3</sub> <sup>b</sup>	25.76	11.90	15.37	17.05	16.72	15.72	13.51	17.03	24.78	14.40	22.31	23.77
FeO <sup>b</sup>	16.52	17.99	13.69	13.64	21.62	18.22	16.30	14.20	18.73	18.99	13.80	12.14
MnO	4.25	13.89	18.58	17.54	6.17	10.51	15.23	16.48	2.59	9.62	12.21	11.75
Na <sub>2</sub> O	10.69	11.75	10.40	9.83	10.88	11.80	11.37	10.51	10.94	12.09	10.13	11.05
Li <sub>2</sub> O <sup>c</sup>	0.40 ± 0.17	n.d.	n.d.	0.11 ± 0.01	n.d.	0.057 ± 0.008	0.18 ± 0.02	0.22 ± 0.02	0.38 ± 0.07	n.d.	n.d.	0.14 ± 0.01
Total	100.83	98.58	101.00	101.10	99.06	99.74	99.83	101.92	101.30	98.03	101.18	101.41
Cation numbers calculated on the basis of 3 P per formula unit												
P	3.000	3.000	3.000	3.000	3.000	3.000	3.000	3.000	3.000	3.000	3.000	3.000
Fe <sup>3+</sup>	1.589	0.737	0.954	1.058	1.021	0.965	0.833	1.045	1.506	0.894	1.392	1.489
Fe <sup>2+</sup>	1.133	1.238	0.944	0.941	1.467	1.244	1.117	0.968	1.265	1.310	0.957	0.845
Mn <sup>2+</sup>	0.295	0.968	1.298	1.226	0.424	0.727	1.058	1.138	0.177	0.673	0.858	0.828
Na	1.700	1.875	1.663	1.572	1.711	1.867	1.807	1.660	1.714	1.934	1.629	1.783
Li	0.132	—	—	0.037	—	0.018	0.059	0.072	0.123	—	—	0.047
Fe <sub>total</sub> /(Fe <sub>total</sub> + Mn)	0.902	0.671	0.594	0.620	0.854	0.752	0.648	0.639	0.940	0.766	0.733	0.738
□	0.150	0.181	0.141	0.166	0.378	0.179	0.125	0.118	0.214	0.188	0.164	0.007

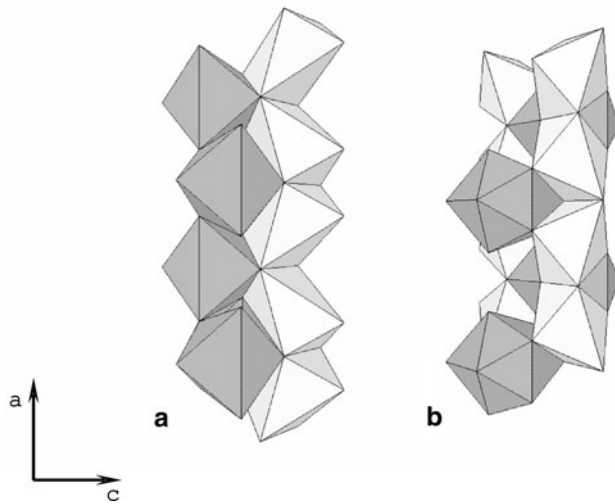
Analyst H.-J. Bernhardt (Bochum, Germany) for the electron-microprobe analyses

<sup>a</sup> Starting material show compositions corresponding to those of the assemblages from the Buranga (BU), Hagendorf-Sid (HA), or Kibingo (KI) pegmatites<sup>b</sup> The FeO and Fe<sub>2</sub>O<sub>3</sub> values have been calculated to maintain charge balance<sup>c</sup> The Li<sub>2</sub>O content was determined by SIMS (Analyst L. Ottolini, Pavia, Italy), and the error represents (1σ) standard deviation

**Table 3** Chemical analyses of triphylite-type phosphates, hydrothermally synthesized from the  $\text{LiNa}_2\text{Mn}_x\text{Fe}^{2+}_{3-x}\text{Fe}^{3+}(\text{PO}_4)_4$  ( $x = 1.054, 1.502, 1.745$ ) starting compositions

Run no.	H.308	H.299	H.152	H.155	H.158	H.310	H.301	H.153	H.156	H.159	H.300	H.309	H.154	H.157	H.160
Number of analyses	(9)	(11)	(13)	(18)	(17)	(10)	(10)	(15)	(14)	(19)	(14)	(13)	(13)	(15)	(18)
Starting material <sup>a</sup>	BU	BU	BU	BU	BU	HA	HA	HA	HA	HA	HA	KI	KI	KI	KI
T (°C)	400	500	600	700	800	400	500	600	700	800	400	500	600	700	800
P <sub>2</sub> O <sub>5</sub>	45.46	45.64	45.42	45.51	44.62	45.69	45.40	45.46	45.43	45.71	44.81	45.32	44.73	44.41	
FeO	14.19	9.82	22.18	25.16	26.86	21.37	20.48	23.24	27.51	29.48	27.29	34.91	32.50	33.91	35.45
MnO	30.08	34.60	23.05	20.66	19.18	22.23	23.79	21.08	18.38	16.30	17.40	10.07	12.69	12.01	11.37
Na <sub>2</sub> O	0.08	0.67	1.08	1.42	1.58	0.04	0.32	1.20	1.35	1.52	0.08	0.16	0.93	1.21	1.25
Li <sub>2</sub> O <sup>b</sup>	9.44 ± 0.46	10.65 ± 0.37	9.25 ± 0.72	8.46 ± 0.85	8.71 ± 0.02	n.d.	9.26 ± 0.57	9.84 ± 0.86	9.17 ± 0.36	7.91 ± 0.27	6.14 ± 0.70	8.94 ± 0.73	n.d.	n.d.	7.93 ± 0.38
Total	99.25	101.38	100.98	101.21	100.95	89.33	99.25	100.82	101.90	99.74	96.62	98.88	91.44	91.86	100.41
Cation numbers calculated on the basis of 1 P per formula unit															
P	1.000	1.000	1.000	1.000	1.000	1.000	1.000	1.000	1.000	1.000	1.000	1.000	1.000	1.000	1.000
Fe <sup>2+</sup>	0.308	0.213	0.482	0.546	0.595	0.462	0.446	0.505	0.597	0.654	0.590	0.770	0.708	0.749	0.789
Mn <sup>2+</sup>	0.662	0.759	0.508	0.454	0.430	0.487	0.524	0.464	0.404	0.366	0.381	0.225	0.280	0.269	0.256
Na	0.004	0.034	0.054	0.072	0.081	0.002	0.016	0.060	0.068	0.078	0.004	0.008	0.047	0.062	0.064
Li	0.987	1.109	0.968	0.883	0.927	—	0.969	1.028	0.957	0.844	0.638	0.948	—	—	0.848
Fe <sub>total</sub> / (Fe <sub>total</sub> + Mn)	0.318	0.219	0.487	0.546	0.580	0.487	0.460	0.521	0.596	0.641	0.608	0.774	0.717	0.736	0.755

Analyst H.-J. Bernhardt (Bochum, Germany) for the electron-microprobe analyses

<sup>a</sup> Starting material show compositions corresponding to those of the assemblages from the Buranga (BU), Hagendorf-Süd (HA), or Kibango (KI) pegmatites<sup>b</sup> The Li<sub>2</sub>O content was determined by SIMS (Analyst L. Ottolini, Pavia, Italy), and the error represents (1 $\sigma$ ) standard deviation**Fig. 2** Diagram showing polyhedral chains in the crystal structures of triphylite (a) and marićite (b). The M(1) sites are in grey; the M(2) sites in white

connected in the *b* direction by sharing edges of their octahedral sites, and the resulting planes are connected in the *c* direction by the PO<sub>4</sub> tetrahedra. Natrophilite, NaM-nPO<sub>4</sub>, is another phosphate with the olivine structure, in which the M(1) site is occupied by Na, while the M(2) site contains the smaller divalent cations (Moore 1972).

The Fe<sub>total</sub>/(Fe<sub>total</sub> + Mn) ratios of the triphylite-type phosphates synthesized in this study were calculated with the empirical correlations established by Fransolet et al. (1984), starting from the calculated unit-cell parameters deposited at Springer's ESM. These ratios are significantly smaller than the Fe<sub>total</sub>/(Fe<sub>total</sub> + Mn) ratios measured with the electron-microprobe (Table 3), and similar correlations, established from the unit-cell parameters reported by Losey et al. (2004) for natural samples of the triphylite-lithiophilite series, do not allow one to calculate Fe<sub>total</sub>/(Fe<sub>total</sub> + Mn) ratios that better match the compositions of Table 3. This feature can be explained by the significant amount of Na that occurs in the synthetic samples investigated herein, an amount which induces an increase of the unit-cell parameters and a decrease of the Fe<sub>total</sub>/(Fe<sub>total</sub> + Mn) ratios calculated from the empirical correlations of the literature.

### Marićite-type phosphates

The hydrothermal experiments realized in the present study have shown the presence of marićite-type phosphates, frequently associated with triphylite and alluaudite at 600 and 700°C (Table 1). Marićite forms large colorless grains reaching 1 mm, with an irregular and frequently rounded shape (Fig. 1b). Identification has been confirmed by X-ray powder diffraction, and the calculated unit-cell parameters

of synthetic marićite-type compounds are deposited at Springer's ESM. The electron-microprobe analyses (Table 4) show  $\text{Fe}_{\text{total}}/(\text{Fe}_{\text{total}} + \text{Mn})$  ratios between 0.56 and 0.83 that are in fairly good agreement with the  $\text{Fe}_{\text{total}}/(\text{Fe}_{\text{total}} + \text{Mn})$  ratios calculated from the unit-cell parameters by using the empirical correlations established by Hatert et al. (2006). The  $\text{Li}_2\text{O}$  content of marićites ranges from 0.22 wt% at 500°C to 0.93 wt% at 600°C (Table 4). The insertion of lithium into the marićite structure, reported here for the first time, is achieved by the replacement of Na, confirmed by the  $(\text{Na} + \text{Li})$  sums clustering around 1.0 (Table 4).

Marićite,  $\text{NaFe}^{2+}(\text{PO}_4)$ , is a natural phosphate described by Sturman et al. (1977) from metamorphic phosphate nodules included in the schists of the Big Fish River area, Yukon, Canada. Le Page and Donnay (1977) described the crystal structure of this mineral ( $a = 6.861(1)$ ,  $b = 8.987(1)$ ,  $c = 5.045(1)$  Å,  $Pmn\bar{b}$ ), which is distinct from the triphylite structure. Whereas the  $Pmn\bar{b}$  type of space group of these two minerals is identical, their unit-cell parameters are significantly different, with  $a/b \sim 0.60$  for triphylite, and  $a/b \sim 0.76$  for marićite (Le Page and Donnay 1977). The marićite structure, more compact than the olivine structure, exhibits chains of edge-sharing  $M(1)$  octahedra, parallel to the  $a$  axis and occupied by  $\text{Fe}^{2+}$ . Each  $M(1)$  octahedron shares faces with the  $M(2)$  polyhedra, which contain 10-coordinated Na (Fig. 2b). In the marićite structure, the  $M(1)$  chains are identical to those of triphylite, but the  $M(2)$  octahedral site is much larger than the  $M(2)$  site of triphylite (Fig. 2).

#### X-phase

In the experiments performed at 800°C, the X-ray powder diffraction patterns show the presence of a phosphate similar to that already obtained by solid-state reaction during the investigation into the  $\text{Na}-\text{Mn}-\text{Fe}^{3+}(+\text{PO}_4)$  system (Hatert 2002), and by hydrothermal synthesis during the investigation into the  $\text{Na}_2(\text{Mn}_{1-x}\text{Fe}_x^{2+})_2\text{Fe}^{3+}(\text{PO}_4)_3$  series (Hatert et al. 2006). This compound, named X-phase by Hatert et al. (2006), occurs as large brownish crystals reaching 1 mm in length; they are elongated and show a good cleavage parallel to their elongation (Fig. 1c, d). Several datasets were collected on a 4-circle diffractometer, in order to solve the crystal structure of this phosphate, but the presence of satellite reflections indicates that its crystal structure is probably modulated. For this reason, the refinements were very poor, with a  $R_1$  factor higher than 12%. The measured unit-cell parameters are  $a = 25.892(4)$ ,  $b = 14.792(5)$ , and  $c = 10.364(2)$  Å, with type of space group  $Pnma$  or  $Pna2_1$ .

The electron-microprobe analyses (Table 4) show chemical compositions similar to those observed by Hatert

et al. (2006), with  $\text{Fe}_{\text{total}}/(\text{Fe}_{\text{total}} + \text{Mn})$  ratios between 0.563 and 0.726. Significant amounts of lithium were detected, evolving from 0.66 wt%  $\text{Li}_2\text{O}$  at 700°C to 1.03–1.17 wt%  $\text{Li}_2\text{O}$  at 800°C. The low totals of the chemical analyses (Table 4) could be related to the presence of  $\text{H}_2\text{O}$  or  $\text{OH}^-$  groups, as previously suggested by Hatert et al. (2006). The unit-cell parameters measured on the samples of X-phase synthesized in this study are deposited at Springer's ESM, and the  $\text{Fe}_{\text{total}}/(\text{Fe}_{\text{total}} + \text{Mn})$  ratios calculated with the correlations established by Hatert et al. (2006) are in fairly good agreement with the chemical data (Table 4).

#### $(\text{Fe},\text{Mn})_3(\text{PO}_4)_2 \cdot n\text{H}_2\text{O}$

A brownish phosphate, forming elongated crystals reaching 50 µm in length, was observed in two runs performed at 600°C (H.152 and H.153; see Table 1). This phase appears dark gray in backscattered electron microscopy, indicating that it certainly contains a significant amount of a low mean-atomic mass component. This suggestion is confirmed by the low totals of the electron-microprobe analyses, ranging from 76.20 to 85.47 wt%. Moreover, qualitative SIMS analyses of H in this matrix allowed one to detect very high  $\text{H}^+$  current intensities of orders of magnitude higher than those relative to  $\text{H}^+$  in the other Li matrixes investigated here. The absence of well-characterized Li-phosphate(s) to be used for H calibration prevented getting quantitative  $\text{H}_2\text{O}$  concentration data in this brownish phosphate. The composition, calculated from the chemical data, is  $(\text{Fe},\text{Mn})_3(\text{PO}_4)_2 \cdot n\text{H}_2\text{O}$ , with a  $\text{Fe}_{\text{total}}/(\text{Fe}_{\text{total}} + \text{Mn})$  ratio between 0.666 and 0.781. Due to the fibrous habit of this phosphate and the impossibility to select a sufficient amount of sample, it was difficult to obtain a good X-ray powder diffraction pattern and to confirm its identification.

#### Magnetite

Magnetite has been observed together with alluaudite, triphylite, and marićite in one run at 600°C (run H.154; see Table 1), and it forms large grains with a white color in backscattered electron microscopy. The electron-microprobe analysis shows a content of 0.17 wt% MnO.

#### Natural alluaudite + triphylite assemblages

In the Hagendorf-Süd pegmatite, Boury (1981) reinvestigated the assemblage triphylite–zwieselite  $[\text{Fe}^{2+}\text{Mn}^{2+}(\text{PO}_4)\text{F}]$ , and the assemblage hagendorfite–wolfeite  $[\text{Fe}_2^{2+}(\text{PO}_4)\text{OH}]$ –arrojadite. In these assemblages, primary triphylite is progressively replaced by zwieselite along its cleavage planes, and hagendorfite forms a “chess-like” texture with primary arrojadite. This texture was

**Table 4** Chemical analyses of marícites and X-phase, hydrothermally synthesized from the  $\text{LiNa}_2\text{Mn}_x\text{Fe}_{3-x}^{2+}\text{Fe}^{3+}(\text{PO}_4)_4$  ( $x = 1.054, 1.502, 1.745$ ) starting compositions

	Marícites				X-phase			
Run no.	H.299 (7)	H.152 (9)	H.155 (15)	H.153 (17)	H.154 (14)	H.157 (13)	H.158 (19)	H.159 (21)
Number of analyses								
Starting material <sup>a</sup>	BU	BU	HA	HA	KI	KI	HA	HA
T (°C)	500	600	700	600	700	700	700	800
P <sub>2</sub> O <sub>5</sub>	41.58	41.59	41.94	41.30	41.84	41.40	41.22	41.70
FeO	31.36	24.45	23.52	28.77	26.84	34.31	32.50	27.47
MnO	10.02	17.03	18.21	12.27	15.05	6.81	9.52	20.58
Na <sub>2</sub> O	16.60	16.98	16.20	16.95	16.33	16.57	16.28	8.02
Li <sub>2</sub> O <sup>b</sup>	0.22 ± 0.15	0.40 ± 0.07	n.d.	0.46 ± 0.04	0.66 ± 0.06	0.93 ± 0.14	0.84 ± 0.09	0.66 ± 0.07
Total	99.78	100.45	99.87	99.74	100.72	100.03	100.36	98.44
Cation numbers								
P	1.000	1.000	1.000	1.000	1.000	1.000	1.000	4.000
Fe <sup>2+</sup>	0.745	0.581	0.554	0.688	0.634	0.819	0.779	2.602
Mn <sup>2+</sup>	0.241	0.410	0.434	0.297	0.360	0.164	0.231	1.975
Na	0.914	0.935	0.884	0.940	0.894	0.917	0.905	1.763
Li	0.025	0.045	—	0.053	0.075	0.107	0.097	0.301
F <sub>Fe</sub> <sub>total</sub> /F <sub>Fe</sub> <sub>total</sub> + Mn)	0.756	0.586	0.561	0.698	0.638	0.833	0.771	0.569
								0.613
								0.726

Analyst H.-J. Bernhardt (Bochum, Germany) for the electron-microprobe analyses

Cation numbers were calculated on the basis of 1 (marícites) or 4 (X-phase) P atoms per formula unit

<sup>a</sup> Starting material show compositions corresponding to those of the assemblages from the Buranga (BU), Hagendorf-Sid (HA), or Kibingo (KI) pegmatites<sup>b</sup> The Li<sub>2</sub>O content was determined by SIMS (Analyst L. Ottolini, Pavia, Italy), and the error represents (1 $\sigma$ ) standard deviation

**Table 5** New chemical analyses of natural alluaudite + triphylite (or heterosite) assemblages

Mineral Sample no. Number of analyses Locality <sup>a</sup>	Triphylite PK-17 HA	Alluaudite HGS-5 HA	Heterosite RGM5469 KI	Alluaudite RGM5469 KI	Triphylite BU83-7 BU	Alluaudite BU83-7 BU
P <sub>2</sub> O <sub>5</sub>	45.76	42.97	44.52	42.94	46.71	44.40
SiO <sub>2</sub>	0.21	0.04	0.06	0.05	0.04	0.03
Al <sub>2</sub> O <sub>3</sub>	0.02	0.02	0.02	0.21	0.01	0.28
Fe <sub>2</sub> O <sub>3</sub> <sup>b</sup>	0.00	15.60	43.54	16.62	25.60	27.88
MgO	0.19	0.57	0.38	0.54	0.65	0.76
FeO <sup>b</sup>	34.25	11.70	1.02	16.20	1.52	0.00
ZnO	0.06	0.03	0.38	0.47	0.17	0.24
MnO	10.54	18.33	6.23	11.41	19.89	20.00
CaO	0.02	1.45	0.04	3.13	0.01	0.43
Na <sub>2</sub> O	0.01	9.35	0.01	7.77	0.02	5.37
K <sub>2</sub> O	0.00	0.00	0.01	0.04	0.00	0.01
Li <sub>2</sub> O <sup>c</sup>	9.80 ± 0.76	0.0100 ± 0.0002	0.089 ± 0.016	0.007 ± 0.0003	5.50 ± 0.35	0.004 ± 0.001
Total	100.86	100.08	96.30	99.39	100.11	99.40
Cation numbers						
P	1.000	3.000	1.000	3.000	1.000	3.000
Si	0.005	0.004	0.002	0.004	0.001	0.002
Al	0.001	0.002	0.001	0.021	0.000	0.027
Fe <sup>3+</sup>	0.000	0.968	0.869	1.032	0.487	1.675
Mg	0.007	0.070	0.015	0.067	0.024	0.090
Fe <sup>2+</sup>	0.739	0.807	0.023	1.118	0.032	0.000
Zn	0.001	0.002	0.008	0.029	0.003	0.014
Mn <sup>2+</sup>	0.230	1.280	0.140	0.797	0.426	1.352
Ca	0.000	0.128	0.001	0.277	0.000	0.037
Na	0.001	1.495	0.000	1.243	0.001	0.831
K	0.000	0.000	0.000	0.004	0.000	0.001
Li	1.018	0.003	0.009	0.002	0.559	0.001
Fe <sub>total</sub> /(Fe <sub>total</sub> ± Mn)	0.763	0.581	0.864	0.730	0.549	0.553
□	0.000	0.245	0.991	0.410	0.441	0.972

Analyst H.-J. Bernhardt (Bochum, Germany) for the electron-microprobe analyses

Cation numbers were calculated on the basis of 3 (alluaudite) or 1 (triphylite, heterosite) P atoms per formula unit

<sup>a</sup> HA Hagendorf-Süd, Germany; KI Kibingo, Rwanda; BU Buranga, Rwanda

<sup>b</sup> The FeO and Fe<sub>2</sub>O<sub>3</sub> values have been calculated to maintain charge balance

<sup>c</sup> The Li<sub>2</sub>O content was determined by SIMS (Analyst L. Ottolini, Pavia, Italy), and the error represents (1σ) standard deviation

interpreted by Boury (1981) as a replacement, but similar textures involving scorzalite [Fe<sup>2+</sup>Al<sub>2</sub>(PO<sub>4</sub>)<sub>2</sub>(OH)<sub>2</sub>] and montebrasite [LiAlPO<sub>4</sub>(OH)] were observed by Lefèvre (2002) in the Rubindi and Kabilizi pegmatites (Rwanda) and interpreted as co-crystallization textures. In the Buranga pegmatite, Héreng (1989) observed a replacement of triphylite by ferrisicklerite, as well as grains of alluaudite included in triphylite and in ferrisicklerite, without any replacement texture. This observation incited Héreng (1989) to consider a primary origin for alluaudite from Buranga. A similar conclusion was published by Fransolet et al. (2004), who observed, in the Kibingo pegmatite, an

assemblage of alluaudite and heterosite forming grains equal in size, with sharp contacts and without any sign of replacement.

New chemical analyses were performed on the samples previously investigated by Boury (1981), Héreng (1989), and Fransolet et al. (2004) (Table 5). These analyses show that the Fe<sub>total</sub>/(Fe<sub>total</sub> + Mn) ratios of the phosphates are similar to those previously reported in the literature. Determination of the lithium contents indicates that the alluaudite (Buranga) and hagendorfite (Kibingo, Hagendorf-Süd) samples can accommodate between 0.004 and 0.010 wt% Li<sub>2</sub>O; the presence of lithium in natural

alluaudite-type phosphates is here reported for the first time. The high  $\text{Fe}_2\text{O}_3$  content and the low  $\text{Li}_2\text{O}$  content of triphylite from Buranga indicate that the analyzed area was probably contaminated by ferrisicklerite.

## Phase relations

Results between 400 and 800°C (NNO,  $P = 1$  kbar)

In order to understand the temperature stability of the alluaudite + triphylite assemblage, hydrothermal experiments were performed at 400, 500, 600, 700, and 800°C, starting from compositions  $\text{LiNa}_2\text{Mn}_x\text{Fe}_{3-x}^{2+}\text{Fe}^{3+}(\text{PO}_4)_4$  ( $x = 1.054, 1.502, 1.745$ ), which represent the ideal compositions of the alluaudite + triphylite assemblages from the Kibingo, Hagendorf-Süd, and Buranga pegmatites, respectively. The pressure was maintained at 1 kbar, and the oxygen fugacity was controlled by the Ni–NiO buffer. The results of these experiments (Table 1) are presented in Fig. 3, which clearly shows that the alluaudite + triphylite assemblage crystallizes at 400 and 500°C, while the association alluaudite + triphylite + marićite appears at 600 and 700°C. Since marićite has never been observed in granitic pegmatites, the boundary between these two domains, at ca. 550°C, corresponds to the maximum temperature that can be reached by the alluaudite + triphylite assemblages in such geological environments.

At 800°C, the formation of the X-phase + triphylite assemblage indicates a strong reduction of the bulk composition. A similar behavior was previously observed by Hatert et al. (2006) in the  $\text{Na}_2(\text{Mn}_{2-2x}\text{Fe}_{1+2x})(\text{PO}_4)_3$  system. The alluaudite + triphylite + marićite + X-phase assemblage, observed at 700°C (Fig. 3), can be explained by the following reaction:  $0.5\text{LiM}^{2+}\text{PO}_4$  (triphylite) +  $3\text{Na}_2\text{M}_2^{2+}\text{Fe}^{3+}(\text{PO}_4)_3$  (alluaudite) +  $1.5\text{H}_2\text{O} = 4.5\text{NaM}^{2+}\text{PO}_4$  (marićite) +  $\text{Li}_{0.5}\text{Na}_{1.5}\text{M}_5^{2+}(\text{PO}_4)_4$  (X-phase) +  $\text{H}_3\text{PO}_4 + 0.75\text{O}_2$  ( $\text{M}^{2+} = \text{Fe}^{2+}, \text{Mn}$ ).

It is noteworthy that lithium plays a significant role in the crystallization of X-phase, since this phosphate can contain up to 1.17 wt%  $\text{Li}_2\text{O}$ , a content significantly higher than the Li contents of alluaudites and marićites (Tables 2, 4).

Variations of chemical composition with temperature: first experimental evidence of sodium incorporation into triphylite

The temperature dependencies of the  $\text{Fe}_{\text{total}}/(\text{Fe}_{\text{total}} + \text{Mn})$  ratios, calculated from the electron-microprobe analyses reported in Tables 2, 3, and 4, clearly show different behaviors, depending on the structural type of the synthesized phosphates (Fig. 4). At 400°C, a strong partitioning

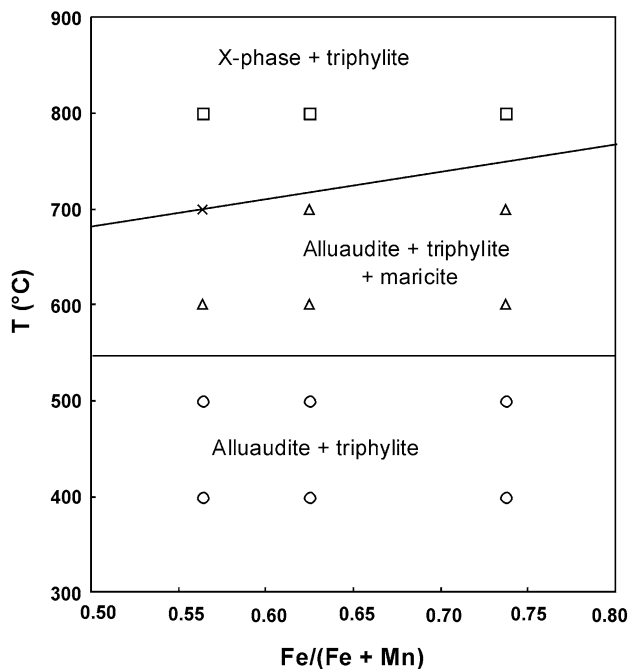


**Fig. 3** Diagram showing the phase relations in the  $\text{LiNa}_2\text{Mn}_x\text{Fe}_{3-x}^{2+}\text{Fe}^{3+}(\text{PO}_4)_4$  ( $x = 1.054, 1.502, 1.745$ ) system, between 400 and 800°C (NNO,  $P = 1$  kbar). Circles = alluaudite, triangles = alluaudite + triphylite + marićite, cross = alluaudite + triphylite + marićite + X-phase, squares = X-phase + triphylite

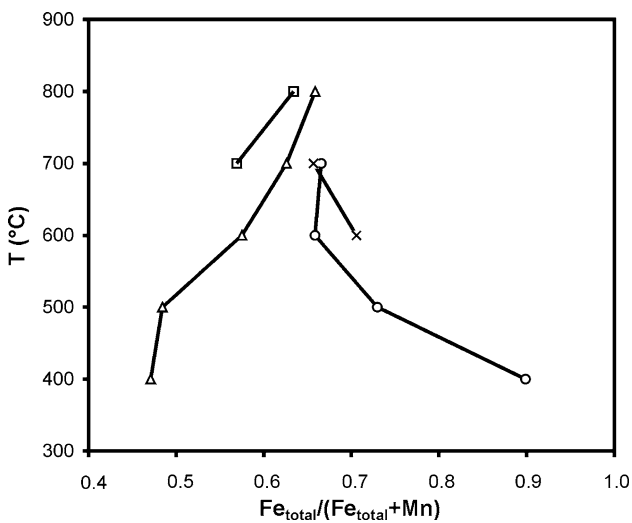


**Fig. 4** Plot showing the temperature dependence of the average  $\text{Fe}_{\text{total}}/(\text{Fe}_{\text{total}} + \text{Mn})$  ratios, for the phosphates synthesized in the  $\text{LiNa}_2\text{Mn}_x\text{Fe}_{3-x}^{2+}\text{Fe}^{3+}(\text{PO}_4)_4$  ( $x = 1.054, 1.502, 1.745$ ) system. Circles = alluaudites, triangles = triphylite, squares = X-phase, crosses = marićite

of Fe and Mn between triphylite and alluaudite is observed, with a low Fe content for triphylite-type phosphates ( $\text{Fe}_{\text{total}}/(\text{Fe}_{\text{total}} + \text{Mn}) = 0.47$ ), and a high Fe content for alluaudite-type phosphates ( $\text{Fe}_{\text{total}}/(\text{Fe}_{\text{total}} + \text{Mn}) = 0.90$ ).

With increasing temperature, this partitioning decreases drastically, as shown by the convergence of the  $\text{Fe}_{\text{total}}/(\text{Fe}_{\text{total}} + \text{Mn})$  ratios of alluaudites and triphylites to a value around 0.65 at 700°C (Fig. 4). The  $\text{Fe}_{\text{total}}/(\text{Fe}_{\text{total}} + \text{Mn})$  ratios of marićites and X-phase show behaviors similar to those of alluaudite- and triphylite-type phosphates, respectively (Fig. 4).

In the investigation into the  $\text{Na}_2(\text{Mn}_{2-2x}\text{Fe}_{1+2x})(\text{PO}_4)_3$  system, Hatert et al. (2006) observed that the  $\text{Fe}_{\text{total}}/(\text{Fe}_{\text{total}} + \text{Mn})$  ratios of alluaudite-type phosphates were relatively constant with temperature. At 400 and 500°C, the runs contained single-phase alluaudites, thus the  $\text{Fe}_{\text{total}}/(\text{Fe}_{\text{total}} + \text{Mn})$  ratios were only constrained by the chemical composition of the starting materials. At 600 and 700°C, the alluaudite + marićite assemblage crystallized, but the low partitioning of Fe and Mn between these two phosphates did not induce a significant change of their  $\text{Fe}_{\text{total}}/(\text{Fe}_{\text{total}} + \text{Mn})$  ratios. In the new experiments reported here, low temperature triphylite-type phosphates are enriched in Mn, when compared with associated alluaudite-type phosphates (Fig. 4). This behavior is certainly due to the presence of large amounts of  $\text{Fe}^{3+}$  in low temperature experiments, while  $\text{Fe}^{2+}$  is more abundant at high temperature, as indicated by the crystallization of the triphylite + X-phase assemblage. Due to crystal-chemical constraints,  $\text{Fe}^{3+}$  can only be hosted by the alluaudite structure, not by the triphylite structure, thus producing a significant Fe-enrichment of alluaudite-type phosphates at low temperatures.

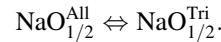
The temperature dependencies of the  $\text{Li}/(\text{Li} + \text{Na})$  ratios (Fig. 5) show that the Li contents of alluaudites, marićites, and X-phase increase progressively with

temperature, while the Li content of triphylite-type phosphates decreases due to the  $\text{Li} \rightarrow \text{Na}$  substitution. Alluaudite- and marićite-type phosphates reach  $\text{Li}/(\text{Li} + \text{Na})$  ratios of 0.04 and 0.10 at 700°C, respectively, while X-phase can accommodate a larger amount of lithium as indicated by a  $\text{Li}/(\text{Li} + \text{Na})$  ratio reaching 0.24 at 800°C. The Na content of triphylite-type phosphates is negligible at 400°C but shows a progressive increase with temperature, up to a  $\text{Li}/(\text{Li} + \text{Na})$  ratio of 0.92 at 800°C (Fig. 5). This incorporation of sodium into the triphylite structure, which is experimentally reported here for the first time, is of particular interest for geothermometric applications. Indeed, minerals of the triphylite–lithiophilite series are the most abundant primary Fe–Mn phosphates in pegmatites, and measurements of their Na content can be easily achieved with the electron-microprobe.

#### Development of a Na-in-triphylite geothermometer

According to Fig. 5, a broad miscibility gap exists between the non-isostructural phases triphylite and alluaudite in the  $\text{LiM}^{2+}\text{PO}_4-2\text{NaM}^{2+}\text{PO}_4-\text{Fe}^{3+}\text{PO}_4$  system. As this gap is temperature dependent, it can generally be used as a geothermometer in cases where triphylite and alluaudite coexist.

For the transformation of a sodium component  $\text{NaO}_{1/2}$  from the alluaudite (All) to the triphylite (Tri) phase, the following reaction can be formulated:



In case of thermodynamic equilibrium, the free enthalpy of reaction equals:

$$\Delta G_{\text{R}} = \Delta H_{\text{R}}^0 - T\Delta S_{\text{R}}^0 + \Delta V_{\text{R}}^0(P - 1) + RT \ln K_{\text{Na}} = 0$$

with the equilibrium constant  $K_{\text{Na}}$ :

$$K_{\text{Na}} = a_{\text{NaO}_{1/2}^{\text{Tri}}}^{\text{Tri}} / a_{\text{NaO}_{1/2}^{\text{All}}}^{\text{All}} = \left( x_{\text{NaO}_{1/2}^{\text{Tri}}}^{\text{Tri}} / x_{\text{NaO}_{1/2}^{\text{All}}}^{\text{All}} \right) \times \left( \gamma_{\text{NaO}_{1/2}^{\text{Tri}}}^{\text{Tri}} / \gamma_{\text{NaO}_{1/2}^{\text{All}}}^{\text{All}} \right)$$

Here,  $a_{\text{NaO}_{1/2}^{\text{Tri}}}$  and  $a_{\text{NaO}_{1/2}^{\text{All}}}$  denote the activity of  $\text{Na}_2\text{O}$  in triphylite and alluaudite and  $\gamma$  as well as  $x$  their activity coefficients and molar ratios. If we assume a constant ratio of the activity coefficients of  $\text{Na}_2\text{O}$  in both phases we get:

$$-(\Delta H_{\text{R}}^0 + \Delta V_{\text{R}}^0(P - 1)) / RT + \Delta S_{\text{R}}^0 / R = \ln K_{\text{NaO}_{1/2}} \\ = \ln \left( x_{\text{NaO}_{1/2}^{\text{Tri}}}^{\text{Tri}} / x_{\text{NaO}_{1/2}^{\text{All}}}^{\text{All}} \right) + \text{const.}$$

In case of pegmatites, the relevant pressures are in the range  $0 \geq P \geq 0.2 \text{ GPa}$ , which is substantially small compared to those of metamorphic rocks. Therefore, we assume that the pressure-dependent contribution to the above equilibrium can be neglected. Consequently, the logarithm of the ratio of the sodium content in coexisting

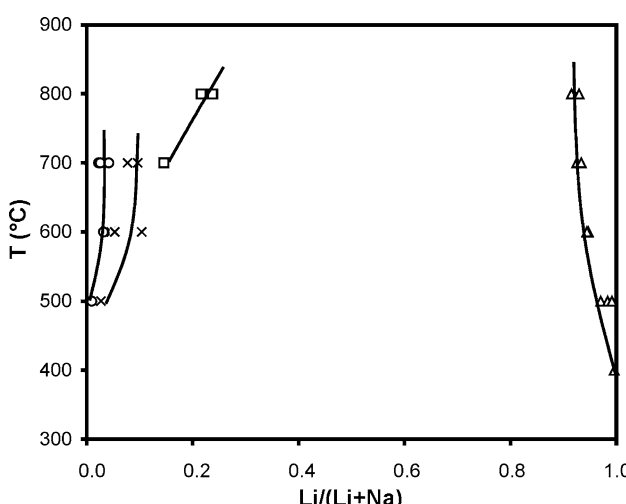


**Fig. 5** Plot showing the temperature dependence of the  $\text{Li}/(\text{Li} + \text{Na})$  ratios, for the phosphates synthesized in the  $\text{LiNa}_2\text{Mn}_x\text{Fe}_{3-x}^{2+}\text{Fe}^{3+}(\text{PO}_4)_4$  ( $x = 1.054, 1.502, 1.745$ ) system. For key see Fig. 4

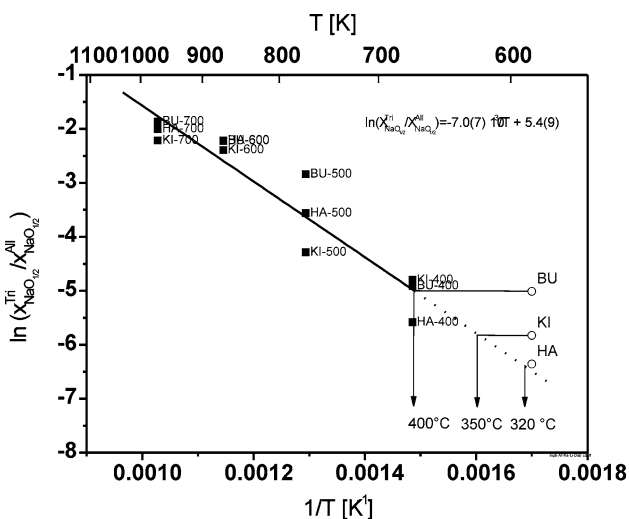


**Fig. 6** Plot of  $\ln(x_{\text{NaO}_{1/2}}^{\text{Tri}}/x_{\text{NaO}_{1/2}}^{\text{All}})$  vs. reciprocal temperature (*lower abscissa*) and temperature (*upper abscissa*) for coexisting alluaudite and triphylite (filled symbols: experimental samples from Tables 2 and 3; open symbols: natural samples from Table 5)

triphylite and alluaudite should scale linearly with reciprocal temperature:

$$\ln\left(x_{\text{NaO}_{1/2}}^{\text{Tri}}/x_{\text{NaO}_{1/2}}^{\text{All}}\right) = -\Delta H_r^0/RT + \Delta S_r^0/R - \text{const.}$$

A fit of these experimental data with the function  $\ln(x_{\text{NaO}_{1/2}}^{\text{Tri}}/x_{\text{NaO}_{1/2}}^{\text{All}}) = a/T + b$  resulted in (Fig. 6):

$$\ln\left(x_{\text{NaO}_{1/2}}^{\text{Tri}}/x_{\text{NaO}_{1/2}}^{\text{All}}\right) = -7.0(7)10^3/T + 5.4(9).$$

This equation can be used to estimate the crystallization temperature of coexisting triphylite and alluaudite.

Principally, this equation can only be applied when triphylite and alluaudite occur in equilibrium, since the maximum sodium content of triphylite depends on the thermodynamic properties of both phases. As can be seen from Fig. 7, the sodium content in triphylite shows the highest values when it is in equilibrium with marićite. The dashed line represents the maximum content of a sodium component in triphylite expressed as wt% Na<sub>2</sub>O and is a linear fit to the maximum Na<sub>2</sub>O content at each temperature. We suggest that the limit of the solubility of a Na<sub>2</sub>O component in triphylite can be used as a rough estimate for the minimum temperature at which a sodium-containing triphylite was equilibrated.

## Discussion

### Stability of the alluaudite + triphylite assemblage

In the present paper, the alluaudite + triphylite assemblage has been obtained experimentally for the first time. This experimental evidence corroborates the primary origin of

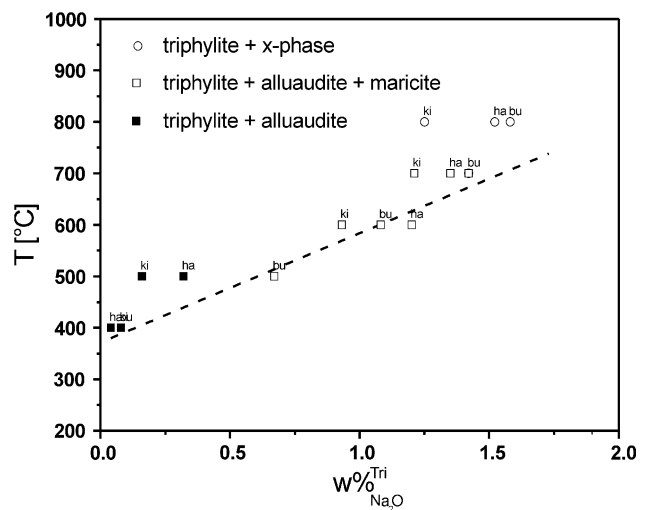


**Fig. 7** Plot showing the maximum solubility of a sodium component (wt% Na<sub>2</sub>O) in triphylite as a function of temperature (experimental samples from Table 3)

the alluaudite + triphylite assemblage in some pegmatites, as for example in the pegmatites from Buranga (Hérent 1989), Hagendorf-Süd (Boury 1981), and Kibingo (Fransolet et al. 2004). Moreover, the phase diagram of Fig. 3 indicates that under an oxygen fugacity controlled by the NNO buffer, marićite appears at 600 and 700°C, thus restraining the alluaudite + triphylite assemblage below ca. 550°C in granitic pegmatites. This temperature range is in good agreement with the experimental data obtained by Hatert et al. (2006) for the Na<sub>2</sub>(Mn<sub>2-2x</sub>Fe<sub>1+2x</sub>)(PO<sub>4</sub>)<sub>3</sub> system, and with the temperatures generally accepted for the formation of primary minerals in rare-element pegmatites (London 2008).

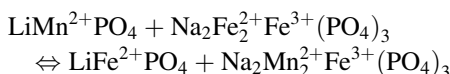
In the Hagendorf-Süd pegmatite, hematite is known to occur included in hagendorfite and triphylite, thus indicating that the oxygen fugacity could be higher than that applied in our experiments. More investigations are needed to answer this question, but the use of a high oxygen fugacity would probably provoke the disappearance of marićite and the replacement of triphylite-type phosphates by Li<sub>3</sub>Fe<sub>2</sub><sup>3+</sup>(PO<sub>4</sub>)<sub>3</sub> (Hatert et al. 2000; Hatert 2002), or by favorite [LiFe<sup>3+</sup>(PO<sub>4</sub>)(OH)] (Schmid-Beurmann and Hatert 2005).

Recently, a new phosphate mineral with composition Na<sub>4</sub>Fe<sub>7</sub>(PO<sub>4</sub>)<sub>6</sub> (triclinic *P*1 or *P*  $\overline{1}$ , *a* = 9.643, *b* = 9.633, *c* = 17.645 Å,  $\alpha$  = 88.26,  $\beta$  = 88.16,  $\gamma$  = 64.83°), was described in the Augustinovka iron meteorite, Ekaterinoslav (now Dnepropetrovsk), Ukraine (IMA No. 2006-006, Burke et al. 2006). The X-ray powder diffraction pattern of this phosphate is similar to that of X-phase, thus indicating that this mineral is probably the natural equivalent of X-phase. According to our experimental data and to those obtained by Hatert et al. (2006), the crystallization

temperature of this mineral can be estimated above 700–800°C (Fig. 3), a temperature which is in good agreement with those occurring in iron meteorites (Wasson 1974). Moreover, the low oxygen fugacity prevailing in iron meteorites is in good agreement with the presence of this  $\text{Fe}^{2+}$ -rich phosphate.

#### Partitioning of Fe and Mn between alluaudite and triphylite

In order to compare the chemical compositions of synthetic alluaudite- and triphylite-type phosphates with those of natural minerals, we calculated the partition coefficients of Fe and Mn between these two compounds. The equilibrium can be expressed by the following exchange reaction and distribution coefficient:



$$K_D = X_{\text{Fe}2+}^{\text{Tri}} \cdot X_{\text{Mn}2+}^{\text{All}} / X_{\text{Mn}2+}^{\text{Tri}} \cdot X_{\text{Fe}2+}^{\text{All}}$$

where  $X_{\text{Fe}2+}^{\text{Tri}}$  refers to the atom fraction  $\text{Fe}^{2+}/(\text{Fe}^{2+}+\text{Mn}^{2+})$  in triphylite, and all the other terms are defined analogously.

The temperature dependence of the partition coefficient shows an increase of  $K_D$  with increasing temperature (Fig. 8). At low temperature, the partitioning is very pronounced, with a strong preference of Mn for the triphylite structure and of Fe for the alluaudite structure, as previously discussed (see Fig. 4). At 800°C, however, the partition coefficients converge to 1.0 (Fig. 8), thus indicating that Fe and Mn play the same crystal-chemical role in both the alluaudite- and triphylite-structure types.

The partition coefficients for the natural alluaudite + triphylite assemblages from the Buranga, Hagedorf-Süd, and Kibingo pegmatites, calculated from the

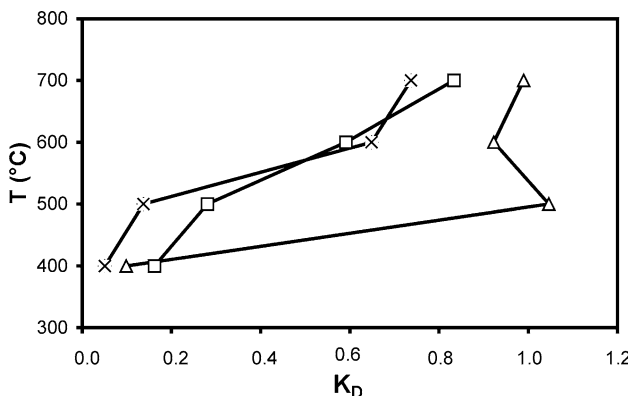


**Fig. 8** Plot showing the temperature dependence of the partition coefficient  $K_D$ , for the phosphates synthesized in the  $\text{LiNa}_2\text{Mn}_x\text{Fe}_{3-x}^{2+}\text{Fe}^{3+}(\text{PO}_4)_4$  system.  $x = 1.054$  (triangles, KI), 1.502 (squares, HA), and 1.745 (crosses, BU)

chemical analyses reported in the literature, are 1.00, 1.67, 2.25, respectively. For the Buranga assemblage, partition coefficients would indicate a crystallization temperature close to 700°C, according to our experimental data (Fig. 8). This temperature is probably overestimated, since the Buranga pegmatite is highly differentiated and of lower temperature, according to its high Mn content. For the Hagedorf-Süd and Kibingo assemblages, the partitioning coefficients were not reproduced experimentally and indicate a preference of iron for the triphylite structure, not for the alluaudite structure. Consequently, the partition coefficients derived from the experimental data cannot be used to calculate reliable temperatures of crystallization for the natural alluaudite + triphylite assemblages.

However, it is noteworthy that the evolution of the partition coefficients follows the degree of pegmatite differentiation. The Buranga assemblage is the Mn-richest, thus indicating that this pegmatite is highly differentiated and of low temperature, according to the general rule that considers a decrease of the  $\text{Fe}_{\text{total}}/(\text{Fe}_{\text{total}} + \text{Mn})$  ratio in isomorphous series of minerals during the pegmatite evolution (Baldwin and Von Knorring 1983; Černý et al. 1985, 1996). On the other hand, the Kibingo assemblage is the Fe-richest, indicating that this pegmatite is poorly differentiated and of high temperature. The partition coefficient  $K_D$  is positively correlated with temperature, thus following the trend established experimentally (Fig. 8). These partition coefficients can consequently be used to classify pegmatites according to their degree of differentiation.

#### Partitioning of Li and Na between alluaudite and triphylite

The results presented in this paper report the first experimental evidence of Na incorporation into triphylite. The chemical analyses of the primary alluaudite + triphylite assemblages from the Buranga, Kibingo, and Hagedorf-Süd pegmatites (see literature data and Table 5) show very low Na contents for triphylite-type phosphates, between 0.00 and 0.03 wt%  $\text{Na}_2\text{O}$  and values for  $\ln(x_{\text{NaO}1/2}^{\text{Tri}}/x_{\text{NaO}1/2}^{\text{All}})$  between –5.5 and –6.5. These values would indicate very low temperatures of crystallization between 320 and 400°C (Tables 2, 3; Fig. 6).

The SIMS analyses of the natural assemblages also indicate that Li occurs in alluaudites, which show  $\text{Li}_2\text{O}$  contents between 0.004 and 0.010 wt% (Table 5). The presence of lithium in natural alluaudite-type phosphates is mentioned in the literature (Moore and Ito 1979), but the high  $\text{Li}_2\text{O}$  contents reported by those authors, up to 0.06 wt%, are certainly due to impurities, difficult to avoid when minerals are mechanically separated for wet-chemical analyses. Our SIMS measurements on natural alluaudites are consequently the first confirmed occurrences of lithium

in these phosphates. A comparison with the Li contents of alluaudite-type phosphates obtained experimentally (Table 2; Fig. 5) indicates a temperature of crystallization below 500°C for natural alluaudites.

The occurrence of lithium in alluaudite-type phosphates is not really surprising, since Hatert et al. (2000, 2002) and Hatert (2004) inserted up to 1 Li *p.f.u.* in the  $(\text{Na}_{1-x}\text{Li}_x)\text{MnFe}_2(\text{PO}_4)_3$ ,  $(\text{Na}_{1-x}\text{Li}_x)\text{CdIn}_2(\text{PO}_4)_3$ , and  $(\text{Na}_{1-x}\text{Li}_x)_{1.5}\text{Mn}_{1.5}\text{Fe}_{1.5}(\text{PO}_4)_3$  solid solutions. These Li-rich alluaudite-type phosphates were synthesized by solid-state reaction methods between 900 and 950°C, thus indicating that high temperatures certainly favor the insertion of lithium in the alluaudite structure. This observation is in good agreement with the experimental results given in the present paper (Fig. 5).

#### Geothermometric applications

The Na-in-triphylite geothermometer, presented in this paper, can easily be applied to natural assemblages. The wet-chemical and electron-microprobe analyses, performed by Fransolet et al. (1984) and Losey et al. (2004) on natural phosphates of the triphylite–lithiophilite series, generally show low sodium contents between 0.01 and 0.05 wt%  $\text{Na}_2\text{O}$ . These Na contents correspond to minimum temperatures between 350 and 400°C, according to Fig. 7. However, two samples analyzed by Fransolet et al. (1984) show significantly higher Na contents: Mg-rich triphylite from Angarf-Sud, Morocco (0.23 wt%  $\text{Na}_2\text{O}$ ), and lithiophilite from Nyiramuganza, Rwanda (0.14 wt%  $\text{Na}_2\text{O}$ ). The temperatures calculated from these Na contents are 400 and 420°C, respectively, but these data have to be used with caution since the samples have probably been contaminated by alluaudite during the wet-chemical analyses.

This first example shows the reliability of the Na-in-triphylite geothermometer, which can be applied to estimate the crystallization temperatures of triphylites. The geothermometer is independent of the minerals associated with triphylite–lithiophilite (Fig. 7), and of the  $\text{Fe}^{2+}/(\text{Fe}^{2+} + \text{Mn})$  ratio of these olivine-type phosphates (Fig. 5). As a consequence, this geothermometer should not be significantly affected by variations of the oxygen fugacity, since the oxygen fugacity mainly controls the  $\text{Fe}^{2+}/\text{Fe}^{3+}$  ratio, and consequently the  $\text{Fe}^{2+}/(\text{Fe}^{2+} + \text{Mn})$  ratio.

In order to obtain reliable temperature data, however, a significant amount of sodium has to be available during the crystallization of triphylite. The presence of primary sodium phosphates associated with triphylite, as for example fillowite, alluaudite, or possibly wyllieite, should be a good indication of the presence of sodium in the primary pegmatitic fluid. In such sodium-rich systems, the slow cooling of Na-rich triphylite would produce exsolutions of a sodium phosphate, as for example alluaudite,

fillowite or marićite. If such exsolutions are observed in pegmatites, the measurement of their proportions should allow one to calculate minimal temperatures of crystallization, according to the phase diagram of Fig. 7.

**Acknowledgments** Many thanks are due to H.-J. Bernhardt, who performed the electron-microprobe analyses at the Ruhr-University of Bochum (Germany), as well as to A.-M. Fransolet, T.L. Grove, J. Webster, and an anonymous reviewer for their constructive comments. FH also thanks the F.N.R.S. (Belgium) for a position of “Chercheur qualifié” and for grants 1.5.113.05.F and 1.5.098.06.F.

#### References

- Baldwin JR, Von Knorring O (1983) Compositional range of Mn-garnet in zoned granitic pegmatites. Can Mineral 21:683–688
- Boury P (1981) Comportement du fer et du manganèse dans les associations de phosphates pegmatitiques. Master thesis, University of Liège, p 118
- Brunet F, Chopin C, Seifert F (1998) Phase relations in the  $\text{MgO}-\text{P}_2\text{O}_5-\text{H}_2\text{O}$  system and the stability of phosphoellenbergerite: petrological implications. Contrib Mineral Petro 131:54–70
- Burke EAJ, Ferraris G, Hatert F (2006) New minerals approved in 2006, nomenclature modifications approved in 2006 by the Commission on New Minerals, Nomenclature and Classification, International Mineralogical Association. <http://pubsites.uws.edu.au/ima-cnmnc/minerals2006.pdf>
- Burnham CW (1991) LCLSQ version 8.4, least-squares refinement of crystallographic lattice parameters. Department of Earth Planetary Sciences, Harvard University, p 24
- Černý P (1991) Rare-element granitic pegmatites. Part I: anatomy and internal evolution of pegmatite deposits. Geosci Canada 18(2):49–67
- Černý P, Ercit TS (2005) The classification of granitic pegmatites revisited. Can Mineral 40:2005–2026
- Černý P, Meintzer RE, Anderson AJ (1985) Extreme fractionation in rare-element granitic pegmatites: selected examples of data and mechanisms. Can Mineral 23:381–421
- Černý P, Ercit TS, Vanstone PT (1996) Petrology and mineralization of the Tanco rare-element pegmatite, Southeastern Manitoba. Field trip guidebook A4, Geological Association of Canada/Mineralogical Association of Canada Annual Meeting, Winnipeg, Manitoba, May 27–29, 1996, p 63
- Eugster HP (1957) Heterogeneous reactions involving oxidation and reduction at high pressures and temperatures. J Chem Phys 26:1760–1761
- Finger LW, Rapp GR (1969) Refinement of the crystal structure of triphylite. Carnegie Inst Wash Yearbook 68:290–292
- Fisher DJ (1958) Pegmatite phosphates and their problems. Am Mineral 43:181–207
- Fontan F (1978) Etude minéralogique et essais expérimentaux sur des phosphates de fer et de manganèse des pegmatites des Jebilet (Maroc) et des Pyrénées (France). PhD thesis, Université Paul-Sabatier, Toulouse, p 250
- Fontan F, Huvelin P, Orliac M, Permingeat F (1976) La ferrisicklérite des pegmatites de Sidi-Bou-Othmane (Jebilet, Maroc) et le groupe des minéraux à structure de triphylite. Bull Soc française Minéral Cristall 99:274–286
- Fransolet A-M (1975) Etude minéralogique et pétrologique des phosphates de pegmatites granitiques. PhD thesis, University of Liège, p 333

- Fransolet A-M (1977) Le problème génétique des alluaudites. Bull Soc française Minéral Cristall 100:348–352
- Fransolet A-M, Antenucci D, Speetjens J-M (1984) An X-ray determinative method for the divalent cation ratio in the triphylite-lithiophilite series. Min Mag 48:373–381
- Fransolet A-M, Abraham K, Speetjens J-M (1985) Evolution génétique et signification des associations de phosphates de la pegmatite d'Angarf-Sud, plaine de Tazenakht, Anti-Atlas, Maroc. Bull Minéral 108:551–574
- Fransolet A-M, Keller P, Fontan F (1986) The phosphate mineral associations of the Tsaobismund pegmatite, Namibia. Contrib Mineral Petrol 92:502–517
- Fransolet A-M, Antenucci D, Fontan F, Keller P (1994) New relevant data on the crystal chemistry, and on the genetical problem of alluaudites and wyllieites. In: Abstracts of the 16th IMA general meeting, Pisa, pp 125–126
- Fransolet A-M, Keller P, Fontan F (1997) The alluaudite group minerals: Their crystallochemical flexibility and their modes of formation in the granite pegmatites. In: Abstracts of the meeting "Phosphates: biogenic to exotic", London
- Fransolet A-M, Fontan F, Keller P, Antenucci D (1998) La série johnsonvilleite-fallowite dans les associations de phosphates de pegmatites granitiques de l'Afrique centrale. Can Mineral 36:355–366
- Fransolet A-M, Hatert F, Fontan F (2004) Petrographic evidence for primary hagendorfite in an unusual assemblage of phosphate minerals, Kibingo granitic pegmatite, Rwanda. Can Mineral 42:697–704
- Geller S, Durand JL (1960) Refinement of the structure of LiMnPO<sub>4</sub>. Acta Cryst 13:325–331
- Hatert F (2002) Cristallochimie et synthèse hydrothermale d'alluaudites dans le système Na-Mn-Fe-P-O: contribution au problème de la genèse de ces phosphates dans les pegmatites granitiques. PhD thesis, University of Liège, p 247
- Hatert F (2004) Etude cristallochimique et synthèse hydrothermale des alluaudites: contribution nouvelle au problème génétique des phosphates de fer et de manganèse dans les pegmatites granitiques et, partant, à celui de l'évolution de ces gisements. Mém Acad royale Sci Belgique, Cl Sci, Coll in-8°, 3ème série XXI: 96 p
- Hatert F, Keller P, Lissner F, Antenucci D, Fransolet A-M (2000) First experimental evidence of alluaudite-like phosphates with high Li-content: the (Na<sub>1-x</sub>Li<sub>x</sub>)MnFe<sub>2</sub>(PO<sub>4</sub>)<sub>3</sub> series (x = 0 to 1). Eur J Mineral 12:847–857
- Hatert F, Antenucci D, Fransolet A-M, Liégeois-Duyckaerts M (2002) The crystal chemistry of lithium in the alluaudite structure: a study of the (Na<sub>1-x</sub>Li<sub>x</sub>)CdIn<sub>2</sub>(PO<sub>4</sub>)<sub>3</sub> solid solution (x = 0 to 1). J Solid State Chem 163:194–201
- Hatert F, Fransolet A-M, Maresch WV (2006) The stability of primary alluaudites in granitic pegmatites: an experimental investigation of the Na<sub>2</sub>(Mn<sub>2</sub>-2xFe<sub>1+2x</sub>)(PO<sub>4</sub>)<sub>3</sub> system. Contrib Mineral Petrol 152:399–419
- Héring P (1989) Contribution à l'étude minéralogique de phosphates de fer et de manganèse de la pegmatite de Buranga, Rwanda. Master thesis, University of Liège, p 101
- Huvelin P, Orliac M, Permingeat F (1972) Ferri-alluaudite calcifère de Sidi-bou-Othmane (Jebilet, Maroc). Notes Serv géol Maroc 32(241):35–49
- Keller P, Von Knorring O (1989) Pegmatites at the Okatjimukuju farm, Karibib, Namibia. Part I: Phosphate mineral associations of the Clementine II pegmatite. Eur J Mineral 1:567–593
- Lahti SI (1981) On the granitic pegmatites of the Eräjärvi area in Orivesi, southern Finland. Geological Survey Finland Bulletin 314: p 82
- Le Page Y, Donnay G (1977) The crystal structure of the new mineral marićite, NaFePO<sub>4</sub>. Can Mineral 15:518–521
- Lefèvre P (2002) Contribution à l'étude minéralogique et pétrographique des associations des phosphates d'aluminium des pegmatites de Rubindi et Kabilizi (Rwanda). Master Thesis, University of Liège, p 58
- London D (2008) Pegmatites. The Canadian Mineralogist, Special Publication 10, p 347
- London D, Wolf MB, Morgan GB, Gallego Garrido M (1999) Experimental silicate-phosphate equilibria in peraluminous granitic magmas, with a case study of the Alburquerque batholith at Tres Arroyos, Badajoz, Spain. J Petrol 40:215–240
- London D, Morgan GB, Wolf MB (2001) Amblygonite-montebrasite solid solutions as monitors of fluorine in evolved granitic and pegmatitic melts. Am Mineral 86:225–233
- Losey A, Rakovan J, Hughes JM, Francis CA, Dyar MD (2004) Structural variation in the lithiophilite-triphylite series and other olivine-group structures. Can Mineral 42:1105–1115
- Mason B (1941) Minerals of the Varuträsk pegmatite. XXIII. Some iron-manganese phosphate minerals and their alteration products, with special reference to material from Varuträsk. Geol Fören Stockholm Förh 63:117–175
- Moore PB (1971) Crystal chemistry of the alluaudite structure type: contribution to the paragenesis of pegmatite phosphate giant crystals. Am Mineral 56:1955–1975
- Moore PB (1972) Natrophilite, NaMnPO<sub>4</sub>, has ordered cations. Am Mineral 57:1333–1344
- Moore PB, Ito J (1979) Alluaudites, wyllieites, arrojadites: crystal chemistry and nomenclature. Mineral Mag 43:227–235
- O'Neill HSC, Pownceby MI (1993) Thermodynamic data from redox reactions at high temperatures. I. An experimental and theoretical assessment of the electrochemical method using stabilized zirconia electrolytes, with revised values for the Fe-“FeO”, Co-CoO, Ni-NiO and Cu-Cu<sub>2</sub>O oxygen buffers, and new data for the W-WO<sub>2</sub> buffer. Contrib Mineral Petrol 114:296–314
- Ottolini L, Bottazzi P, Vannucci R (1993) Quantification of lithium, beryllium and boron in silicates by secondary ion mass spectrometry using conventional energy filtering. Anal Chem 65:1960–1968
- Ottolini L, Camara F, Hawthorne FC, Stirling J (2002) SIMS matrix effects in the analysis of light elements in silicate minerals: Comparison with SREF and EMPA data. Am Mineral 87:1477–1485
- Roda Robles E, Fontan F, Pesquera Pérez A, Keller P (1998) The Fe-Mn phosphate associations from the Pinilla de Fermoselle pegmatite, Zamora, Spain: occurrence of kryzhanovskite and natrodufrénite. Eur J Mineral 10:155–167
- Roda E, Fontan F, Pesquera A, Velasco F (1996) The phosphate mineral association of the granitic pegmatites of the Fregeneda area (Salamanca, Spain). Mineral Mag 60:767–778
- Schmid-Beurmann P, Hatert F (2005) Experimental Fe<sup>2+</sup>-oxidation in triphylite, LiFePO<sub>4</sub>: possible formation of ferricklerite and heterosite. Berichter der Deutschen Mineralogischen Gesellschaft, Beihefte zum. Eur J Mineral 17:118
- Sturman BD, Mandarino JA, Corlett MI (1977) Marićite, a sodium iron phosphate from the Big Fish River area, Yukon Territory, Canada. Can Mineral 15:396–398
- Tuttle OF (1949) Two pressure vessels for silicate-water studies. Geol Soc America Bull 60:1727–1729
- Wasson JT (1974) Meteorites: classifications and properties. Springer, New York 327 p
- Yakubovich OV, Simonov MA, Belov NV (1977) The crystal structure of a synthetic triphylite, LiFe[PO<sub>4</sub>]. Sov Phys Dokl 22:347–350